Tevatron Run-II Beam Collimation System Performance*

A.I. Drozhdin, N.V. Mokhov, L.Y. Nicolas, D.A. Still, S.I. Striganov

Fermi National Accelerator Laboratory

P.O. Box 500, Batavia, Illinois 60510

July 14, 2004

Abstract

Detailed simulations were performed on beam loss rates in the vicinity of the Tevatron CDF and DØ detectors at the Tevatron Run-II beam collimation system operation and due to beam-gas nuclear elastic interactions [1]. Two optional schemes for antiproton beam collimation are considered.

1 Introduction

Even in good operational conditions in an accelerator, some particles leave the beam core producing a beam halo. This happens because of beam-gas interactions, intra-beam scattering, proton-antiproton collisions in the interaction regions (IP), and particle diffusion due to RF noise, ground motion and resonances excited by the accelerator magnet nonlinearities and power supplies ripple. As a result of halo interactions with limiting apertures, hadronic and electromagnetic showers are induced in accelerator and detector components causing excessive backgrounds in the detectors. Only with a very efficient beam collimation system can one reduce uncontrolled beam losses in the machine to an allowable level. About 0.1% of protons and antiprotons hitting the collimators are scattered back into the beam pipe and later are lost on limiting apertures, in most cases upstream of the CDF and DØ collider detectors. A multi-turn particle tracking through the accelerator with halo interactions with the collimators is conducted with the STRUCT code [2]. All the lattice components with their real strengths and aperture restrictions are taken into account. It is assumed in this study that 3×10^7 protons per second [1] is intercepted by the collimatin system. The 2/3 of this particles interact first with horizontal and the rest with vertical jaws of the primary collimator.

2 Run II Collimation System

The current Run II collimation system is slightly differ from the initial design (Ref. [3]). For each (proton and antiproton) beam, the system consists of a thin primary collimator and two secondary collimators placed at optimal phase advances with respect to the primary ones. As a result of a random kick generated in primary collimator, the halo particle impact parameter drastically increases from $\sim 1\ \mu m$ at the primary collimator to $\sim 100 \mu m$ at the secondary collimators. This decreases

*Work supported by the Universities Research Association, Inc., under contract DE-AC02-76CH00300 with the U. S. Department of Energy.

number of particles outscatterd from the secondary collimators, resulting in a high collimation efficiency. This also decreases secondary collimator jaws heating and mitigates their alignment requirements. The β-functions, dispersions and phase advances at the collimators are presented in Table 1. Collimator locations in the Tevatron ring are shown in Fig. 1. The 5-mm thick tungsten primary collimators are positioned at 5σ from the beam axis both in vertical and horizontal planes. The 1.5-m long stainless steel secondary collimators consist of L-shape jaws placed at 6σ from the beam axis in both horizontal and vertical planes. The proton and antiproton beams position with respect to the primary and secondary collimators are shown in Fig. 2 and Fig. 3. Numerical simulations are done for the Tevatron [4, 5] in the presence of the proton and antiproton orbit separation designed for Run II.

Table 1: β-functions, dispersions and phase advances between primary and secondary collimators for two optional schemes of antiproton beam collimation.

Collimator	β-function (m)		Dispersion (m)	Phase advance between primary and secondary collimators (deg)	
	horizontal	vertical		horizontal	vertical
proton collimators					
D49 primary (p)	84.8	74.0	1.84	0	0
E03 secondary (p)	96.4	58.6	2.38	45	41
F172 secondary (p)	87.0	35.9	5.65	339	341
antiproton collimators (first option)					
F49 primary ($\overline{p}$)	184.4	40.7	2.52	0	0
F48 secondary ($\overline{p}$)	102.2	30.0	1.73	14	48
D172 secondary ($\overline{p}$)	64.0	51.5	4.92	320	337
antiproton collimators (second option)					
F173 primary ($\overline{p}$)	63.0	49.7	4.89	0	0
F171 secondary ($\overline{p}$)	96.0	31.3	5.99	8	15
E02 secondary ($\overline{p}$)	92.9	61.1	2.37	301	315

3 Simulations of Beam Loss at Collimation System Operation

Horizontal and vertical phase space at the proton and antiproton primary and secondary collimators are presented in Fig. 4, 5 and 6. Large amplitude protons are intercepted by the secondary collimators during the first turn after interaction with the primary collimator. Protons (antiprotons) with amplitudes smaller than 6σ survive during several tens of turns until they increase amplitude in next interactions with primary collimators. These particles produce a secondary halo and occupy the 6σ envelope. In Tevatron, beam halo particles interact with primary collimators 2.2 times on average.

3.1 Effect of Secondary Collimators Offset to the CDF and DØ Detectors Background

Next to the collimators limiting apertures in the Tevatron are Roman Pots of the DØ and CDF forward detectors sitting at $\sim 10\sigma_{x,y}$. Halo interactions with Roman Pots can contribute to undesirable backgrounds in the main detectors. The secondary halo hit rate in the Roman Pots depends on

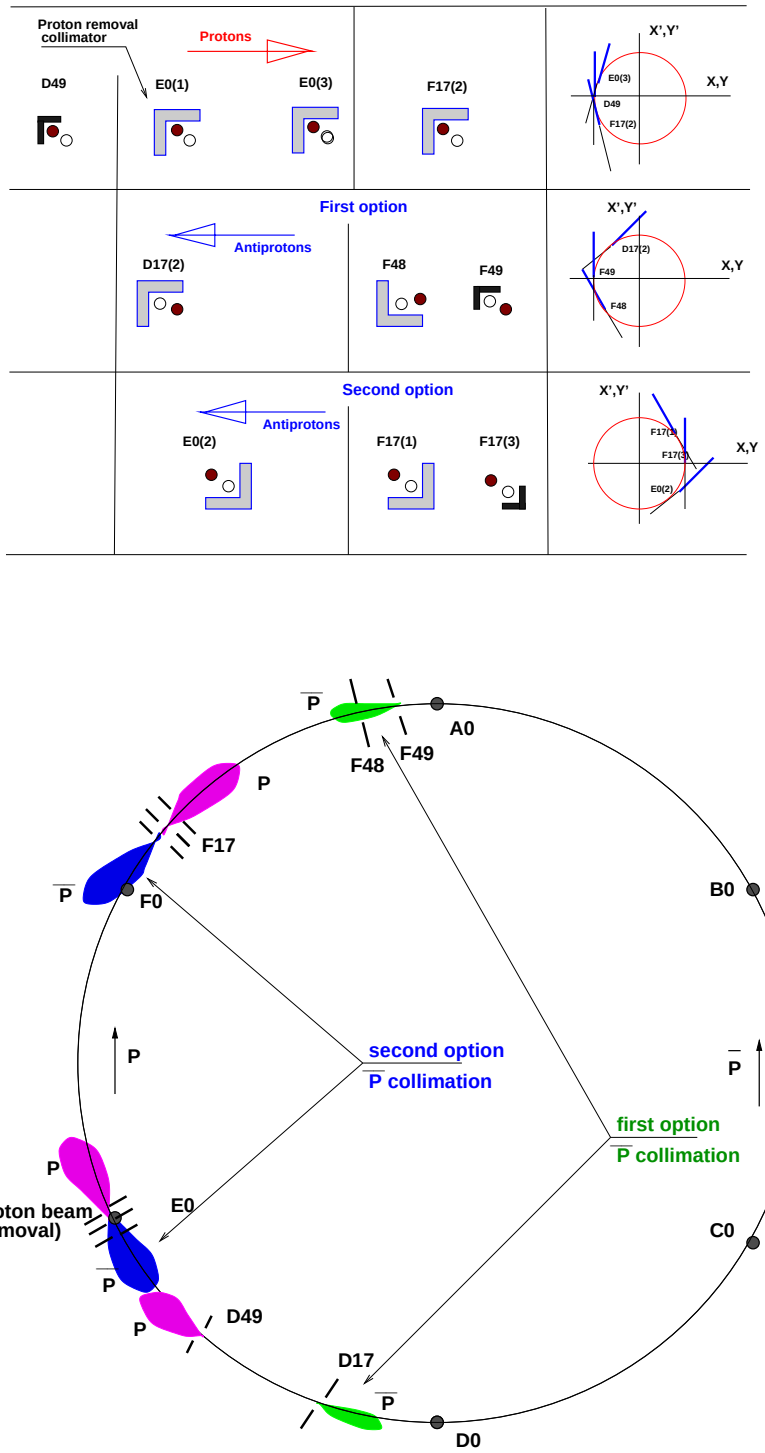

Figure 1: Tevatron Run-II beam collimation system with two optional schemes for antiproton beam collimation.

the secondary collimators offset with respect to the primary one. Calculated beam loss distributions with secondary collimators at different offset are shown in Fig. 7, 8 and 9 for proton beam collimation.

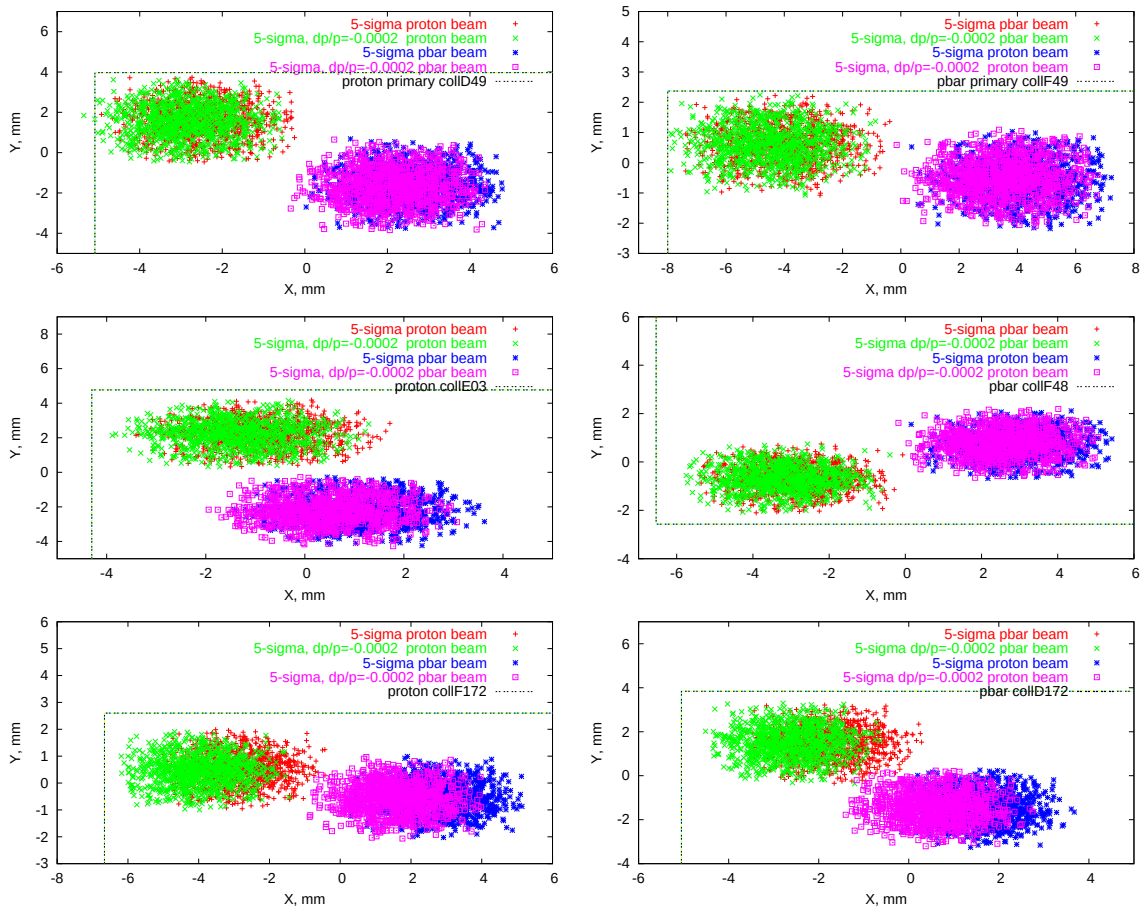

Figure 2: The $5-\sigma$ proton (red (black)) and antiproton (green (grey)) spatial distributions. *Left:* at proton primary collimator D49 (top) and secondary collimators E03 (middle) and F172 (bottom). *Right:* at antiproton primary collimator F49 (top) and secondary collimators F48 (middle) and D172 (bottom) (first option).

Beam loss distributions for antiproton beam collimation with primary collimator F49 and secondary collimators F48 and D17(2) (first option of antiproton beam collimation) are show in Fig. 10. In the second option of antiproton beam collimation (Fig. 11) the second secondary collimator E0(2) is located father from the DØ IP, that permits to reduce background at DØ .

The secondary collimator E0(2) is still to close to the DØ detector. Large number of particles outscattered from this collimator are lost in the last magnets and separators upstream of DØ IP. This losses are proportional to the loss rate in the collimator and can be decreased by retracting this collimator by additional $0.6\sigma_x$, as shown in Fig. 12.

In the third option of aniproton beam collimation a horizontal collimation is done by the F49 primary and F48 and D17(2) secondary collimators, but vertical collimation is done by F17(3) primary and F17(1) and E0(2) secondary collimators. This permits to use horizontal collimators located from inside of the circulating beam, which seems is better for collimation, and use vertical collimators located in optimal phase advances. Beam loss distribution in the DØ and BØ regions for antiproton beam with primary collimators at $5\sigma_{x,y}$ and secondary collimators offset of $1\sigma_{x,y}$ with respect to the primary one are shown for all three options in Fig. 13. The same distributions are

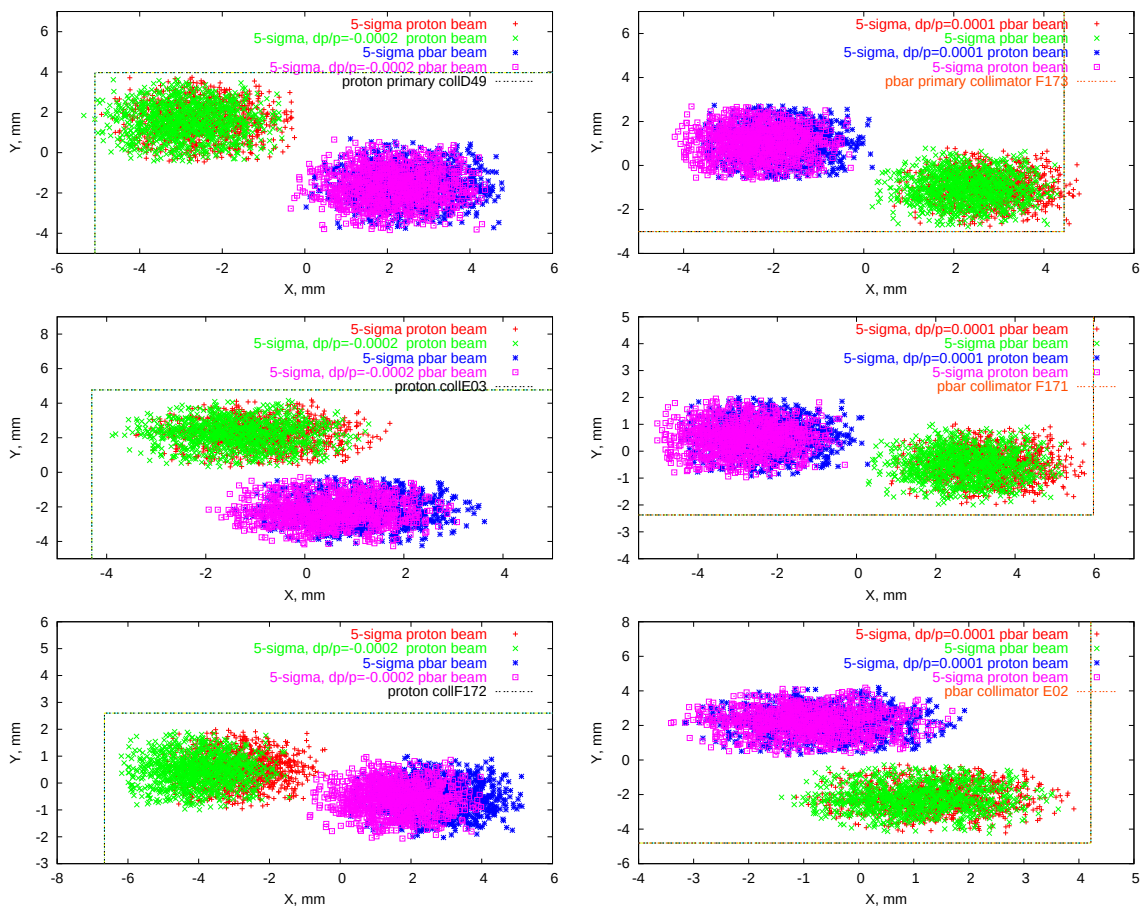

Figure 3: The $5-\sigma$ proton (red (black)) and antiproton (green (grey)) spatial distributions. *Left:* at proton primary collimator D49 (top) and secondary collimators E03 (middle) and F172 (bottom). *Right:* at antiproton primary collimator F173 (top) and secondary collimators F171 (middle) and E02 (bottom) (second option).

presented in Fig. 14 and 15 for additional offset of $0.6\sigma_{x,y}$ in the second secondary collimator. As shown in these figures the second option of collimation with F17(3) primary and F17(1) and E0(2) secondary collimators gives a factor of 2-3 reduction of backgrounds in the detectors.

Normally, the beam scraping is done by the primary collimators at $5\sigma_{x,y}$ and secondary ones at $6\sigma_{x,y}$ at the beginning of accelerator cycle flat top after beams are brought to collisions. After the scraping is done, all collimators are retracted back from the beam by 1 mm, which is approximately equal to $2\sigma_{x,y}$. Beam loss distribution in the DØ and BØ regions for proton beam and for second option of antiproton collimation with primary collimators at $5\sigma_{x,y}$ and secondary at $6\sigma_{x,y}$ are shown in Fig. 16 compared to situation after retracting of collimators by 1 mm from this position. This procedure increases losses in the IPs by a factor of 2-3.

3.2 Possible solutions of antiproton beam collimation.

There are two disadvantages in the existing (first option) collimation system for antiproton direction:

First - the secondary collimator F48 (see Fig. 5) does not work during the first turn after particle interactions with the primary collimator because the vertical jaw of this collimator is positioned on

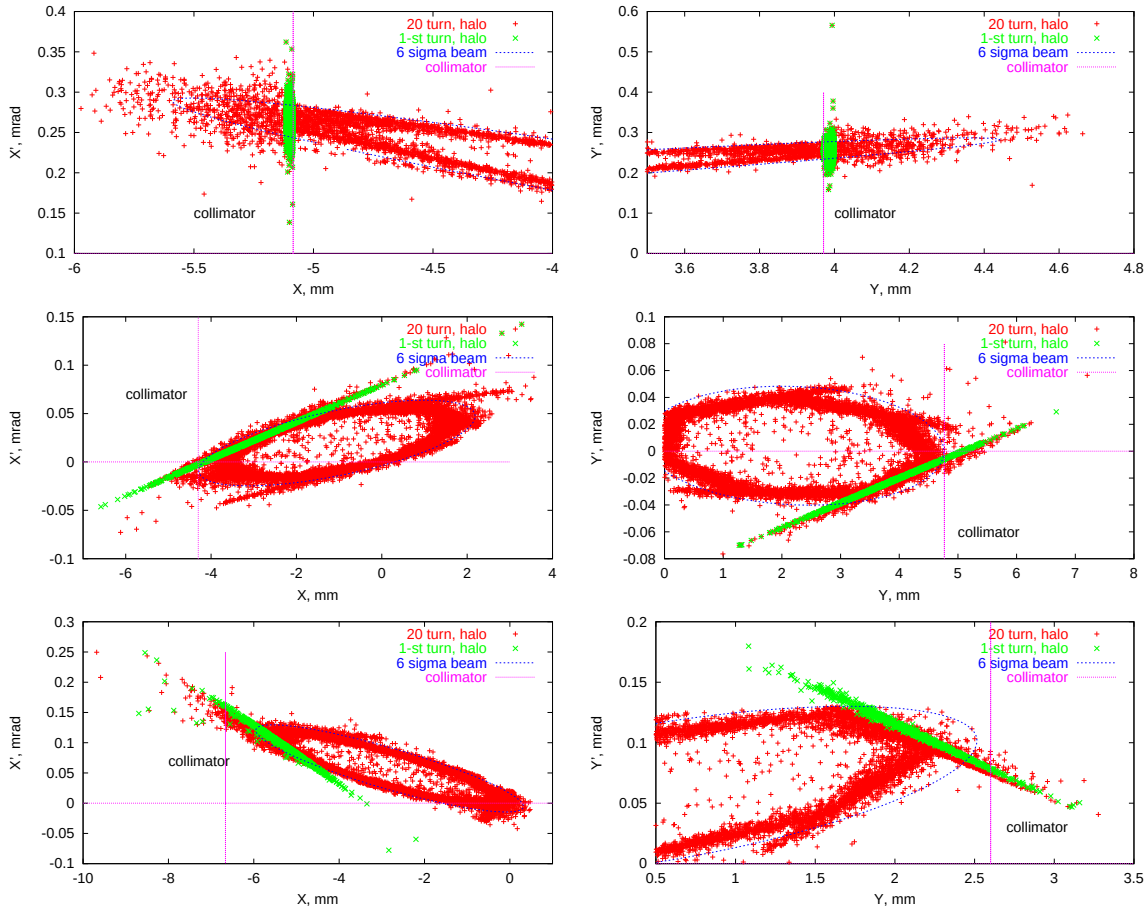

Figure 4: Horizontal (left) and vertical (right) phase space at primary proton collimator D49 (top), and secondary collimators E03 (middle) and F172 (bottom). Green (grey) – halo particles at the first turn after interaction with the primary collimator, red (black) – secondary halo, blue (black line) – 6σ envelope.

the bottom from the beam, but halo particles scattered by the primary collimator are located on the top side of the circulating beam. This jaw can not be placed from the top because of inconvenient sign of beam separation (see Fig. 2). This collimator may work only at the next turns after the first one. But large amplitude particles of halo will be lost in the accelerator mostly in the IPs during the first turn affecting the system efficiency.

Second - secondary collimator D172 is very close to DØ IP. Most of particles outscattered from this collimator are lost in the region of 200 m behind the collimator with big losses in the last magnets and separators upstream of DØ IP. This losses are proportional to the loss rate in the collimator D172 as shown at the bottom of Fig. 17.

The second option of collimation system with F173 primary and F171 and E02 secondary collimators has disadvantage as well:

First - the horizontal collimators are located from outside of the circulating beam. They collimate particles with positive deviation of momentum. Particles with negative deviation of momentum will be collimated in half of synchrotron oscillation than negative deviation gets into positive one. This slow down the process of particle collimation, but should not effect the collimation efficiency.

Second - a particle passed through the primary collimator loose some fraction of the momentum

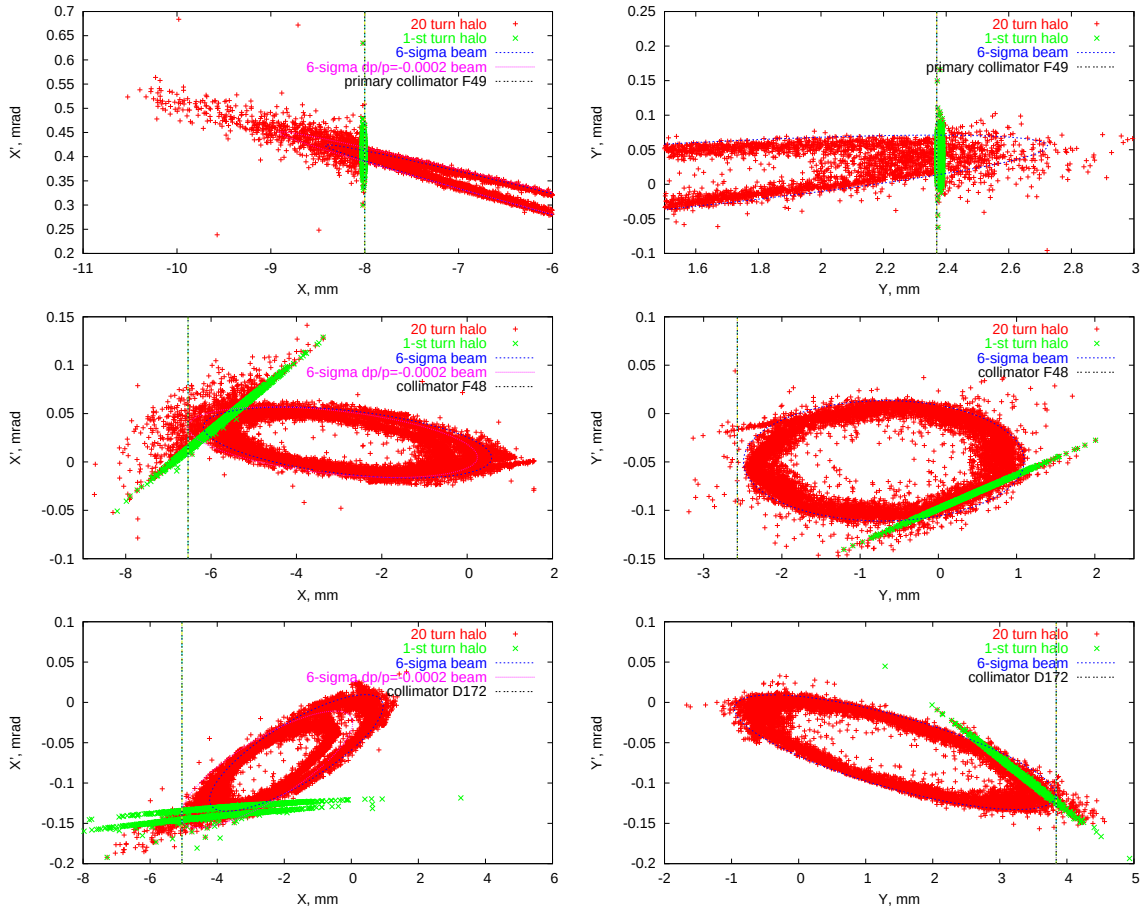

Figure 5: Horizontal (left) and vertical (right) phase space at primary antiproton (first option) collimator F49 (top), and secondary collimators F48 (middle) and D172 (bottom). Green (grey) – halo particles at the first turn after interaction with the primary collimator, red (black) – secondary halo, blue (black line) – 6σ envelope.

and, because the dispersion is positive in the Tevatron, particle change its closed orbit by $dX = D \times dP/P$ and moves inside (far from the collimators jaws). This causes a redistribution of particle halo during collimation. Possibly this may effect additional losses of these particles in the IP regions where dispersion is equal to zero.

3.3 Possible Solutions for Reduction of Background in the Detectors due to Beam-Gas Nuclear Elastic Interactions

Residual gas pressure distribution in the Tevatron has been measured by Bruce Hanna [6]. As shown in Fig. 18 the rate of beam-gas interactions is proportional to the gas pressure. Because of this the background in the detectors depends on average pressure in the accelerator and most of all on the gas pressure in the region of several hundred meters preceding the IP. The reduction of residual gas pressure in the Tevatron C- and D-sectors down to $1-2\times10^{-10} tor$ may effect background reduction at DØ by a factor of 2-5.

Another way of background reduction is a shadow collimators installation at $10-15\sigma_{x,y}$ at A48 and C48 regions upstream of the last three dipoles preceding the CDF and DØ detectors for proton beam and shadow collimators at B17 and D17 regions for antiproton beam. As shown in Fig. 19

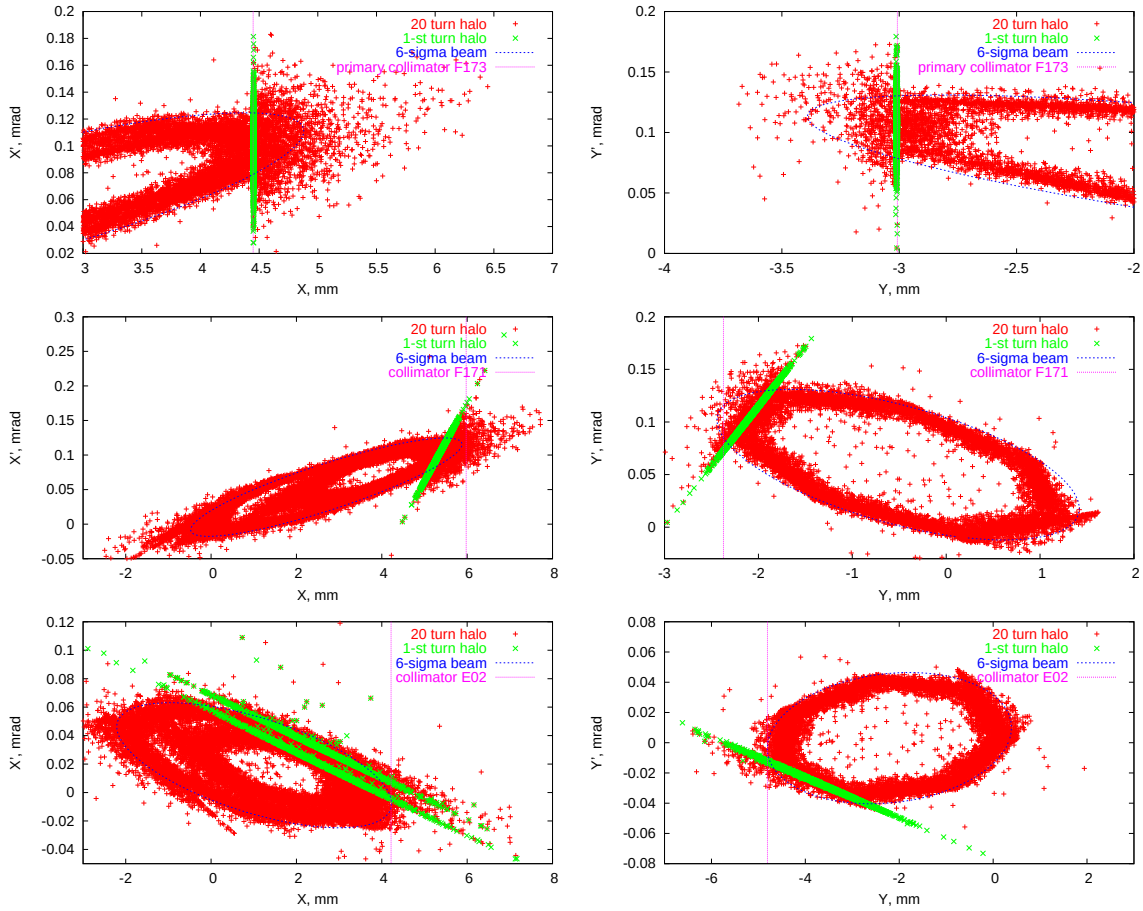

Figure 6: Horizontal (left) and vertical (right) phase space at primary antiproton (second option) collimator F173 (top), and secondary collimators F171 (middle) and E02 (bottom). Green (grey) – halo particles at the first turn after interaction with the primary collimator, red (black) – secondary halo, blue (black line) – 6σ envelope.

and 20 the proton A48 and C48 collimators are much more efficient compared to the antiproton B17 and D17 collimators because of closer location to the detectors.

4 Conclusions

The second option of antiproton beam collimation with F173 primary and F171 and E02 secondary collimators gives better results in background suppression compared to the existing collimation system with primary collimator F49 and secondary collimators F48 and D17(2).

According to simulations the retracting of collimators by 1 mm from their working positions after collimation of the beam at the beginning of collisions increases losses in the IPs by a factor of 2-3. This effect may be reduced by optimizing this offset and secondary collimators offset with respect to the primary one.

The reduction of residual gas pressure in the Tevatron C- and D-sectors down to $1-2\times10^{-10}tor$ may effect nuclear elastic beam-gas scattering related backgrounds reduction at DØ by a factor of 2-5 from proton and antiproton beam.

Another way of background reduction is a shadow collimators installation at $10-15\sigma_{x,y}$ at C48 region upstream of the last three dipoles preceding the DØ detector for proton beam and shadow collimators at B17 and D17 regions for antiproton beam.

References

[1] A.I. Drozhdin, V.A. Lebedev, N.V. Mokhov, L.Y. Nicolas, D.V. Sidorov, S.I. Striganov, A.V. Tollestrup, "Beam Loss and Backgrounds in the CDF and DØ Detectors due to Nuclear Elastic Beam-Gas Scattering", FERMILAB-FN-734, April 2003.

[2] I.S. Baishev, A.I. Drozhdin, N.V. Mokhov, "STRUCT Program User's Reference Manual", SSCL–MAN–0034 (1994); http://www-ap.fnal.gov/∼drozhdin/

[3] M.D. Church, A.I. Drozhdin, A. Legan, N.V. Mokhov, R.E. Reilly, "Tevatron Run-II Beam Collimation System", *Proc. 1999 Particle Accelerator Conf.*, pp. 56-58, New York, March 29 - April 2, 1999; also Fermilab-Conf-99/059 (1999).

[4] M. Martens, Tevatron Run-II Lattice. http://www-ap.fnal.gov/ martens/mad/tevatron/run2/lattice.html.

[5] J.A. Johnstone, Tevatron optics with magnet moves for Roman pots at CDF, FERMILAB-TM-2157, Aug 2001.

[6] B. Hanna, Residual Gas Pressure Measurements, August 2002.

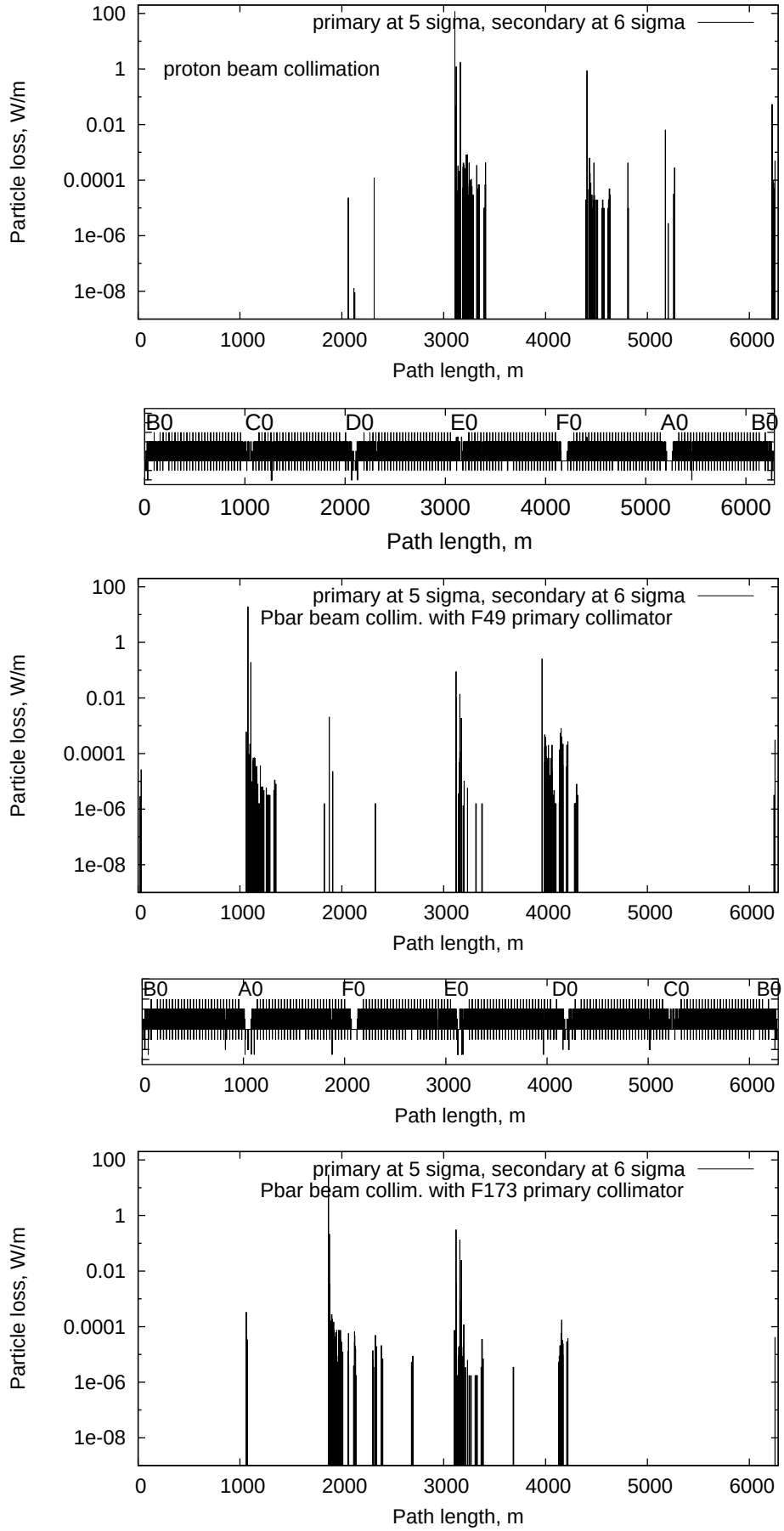

Figure 7: Beam loss distribution in the entire ring for $1\sigma_{x,y}$ secondary collimators offset with respect to the primary one. Top - for proton, middle - for antiproton with primary F49 collimator (first option) and bottom - for antiproton beam with primary F173 collimator (second option).

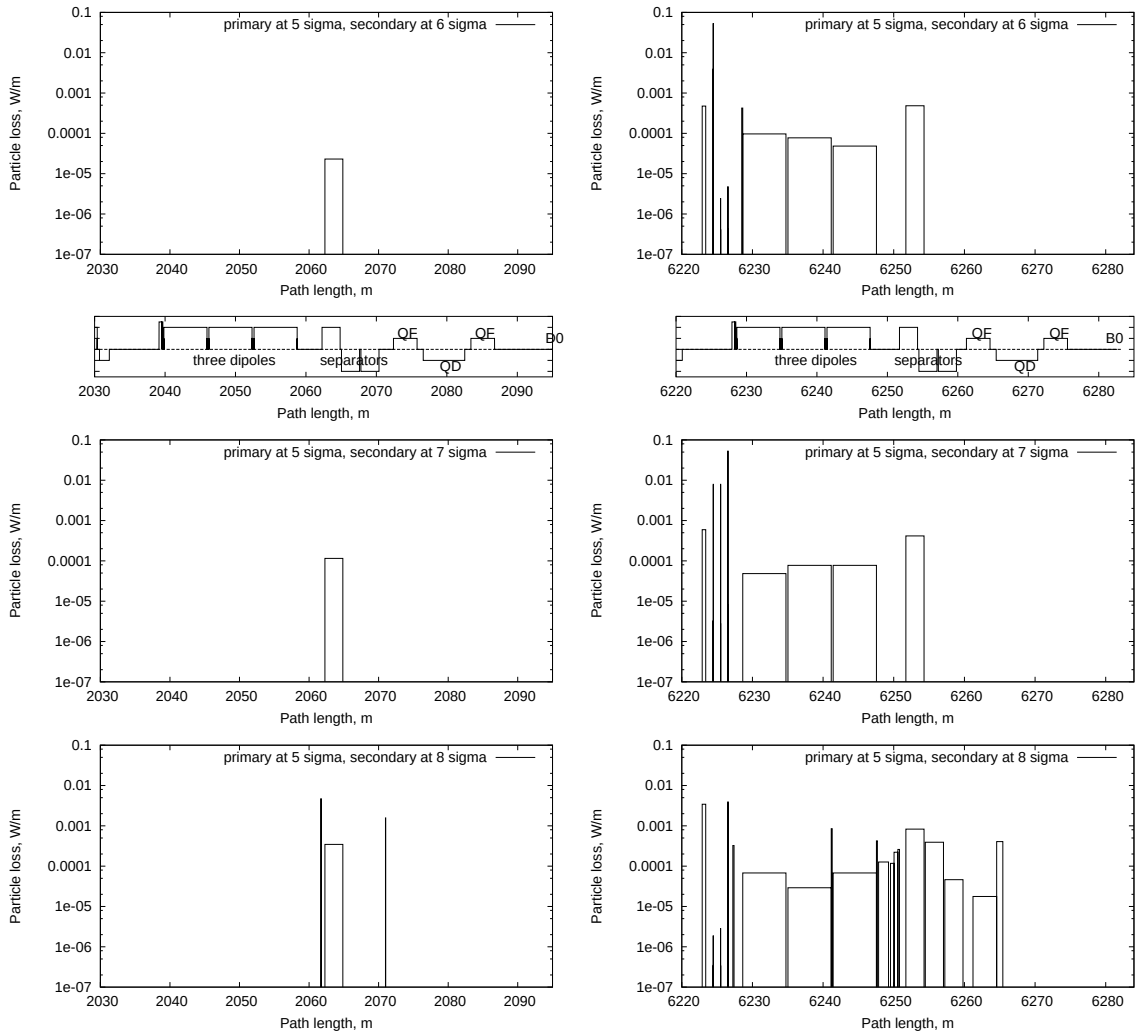

Figure 8: Beam loss distribution in the DØ and BØ regions for proton beam with secondary collimators offset with respect to the primary one of $1\sigma_{x,y}$ (top), $2\sigma_{x,y}$ (middle) and $3\sigma_{x,y}$ (bottom).

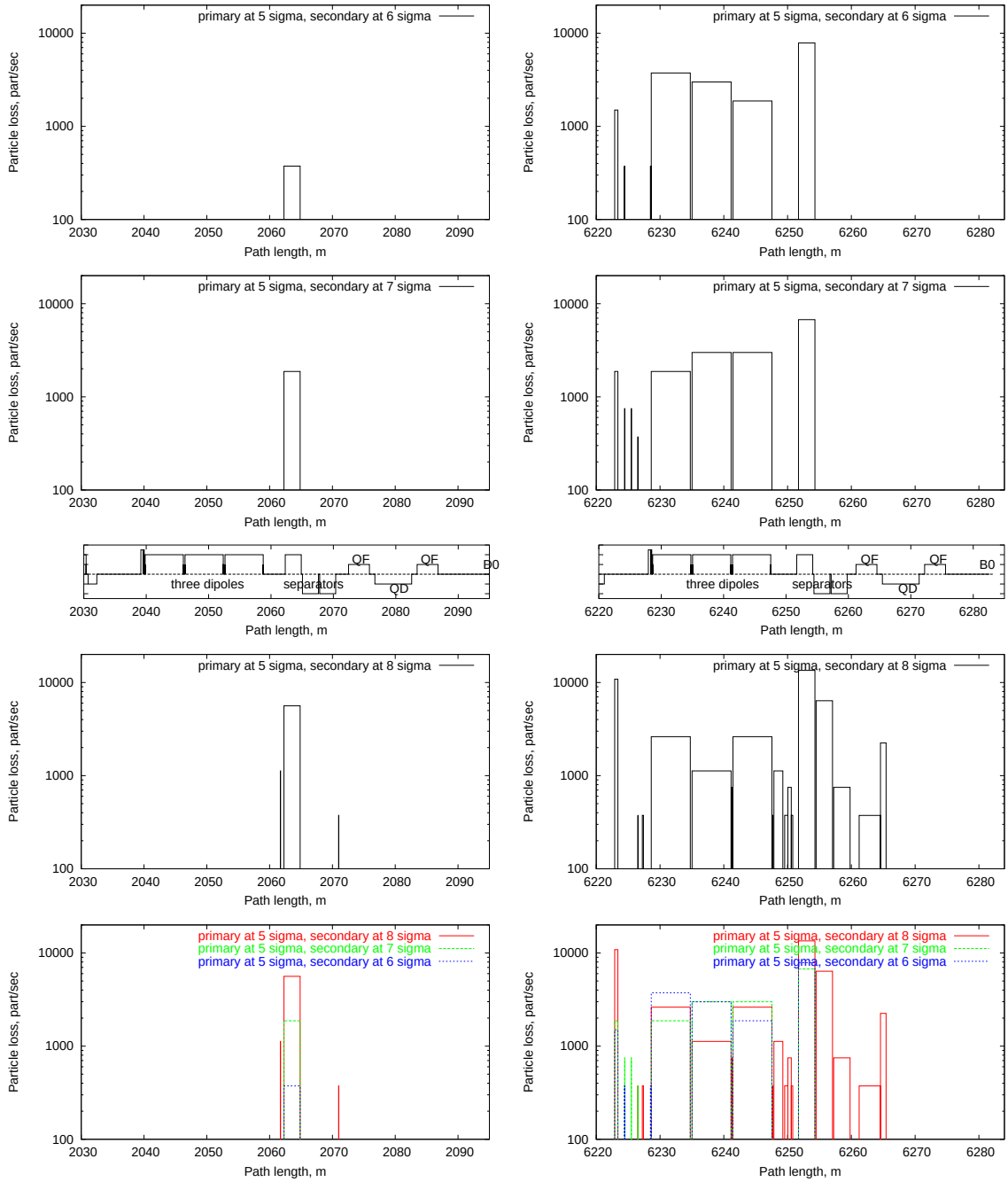

Figure 9: Beam loss distribution in the DØ and BØ regions for proton beam with secondary collimators offset with respect to the primary one of $1\sigma_{x,y}$ (top), $2\sigma_{x,y}$ (second line), $3\sigma_{x,y}$ (4-th line) and comparison of all cases (bottom).

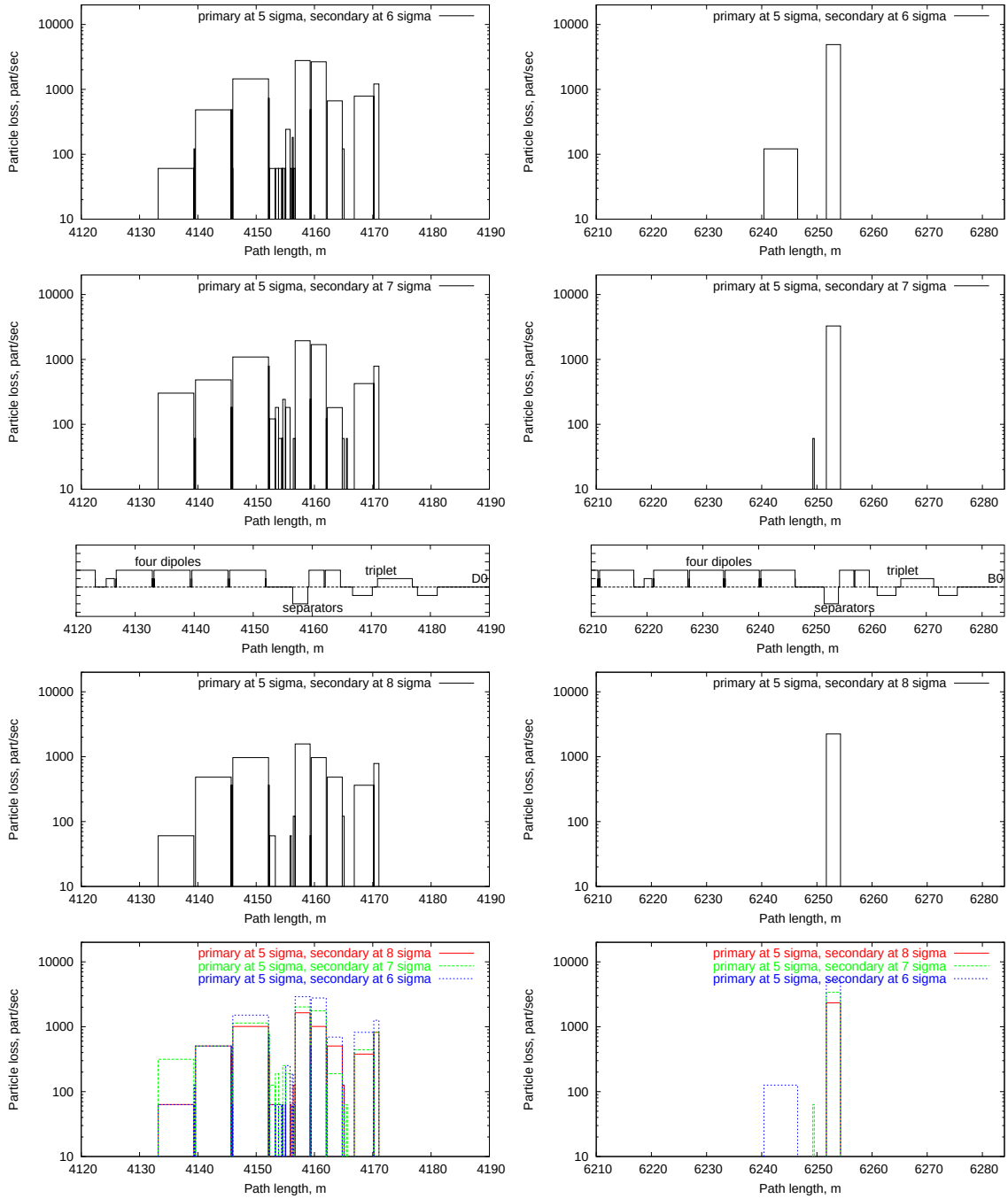

Figure 10: Beam loss distribution in the DØ and BØ regions for antiproton beam (first option) with secondary collimators offset with respect to the primary one of $1\sigma_{x,y}$ (top), $2\sigma_{x,y}$ (second line), $3\sigma_{x,y}$ (4-th line) and comparison of all cases (bottom).

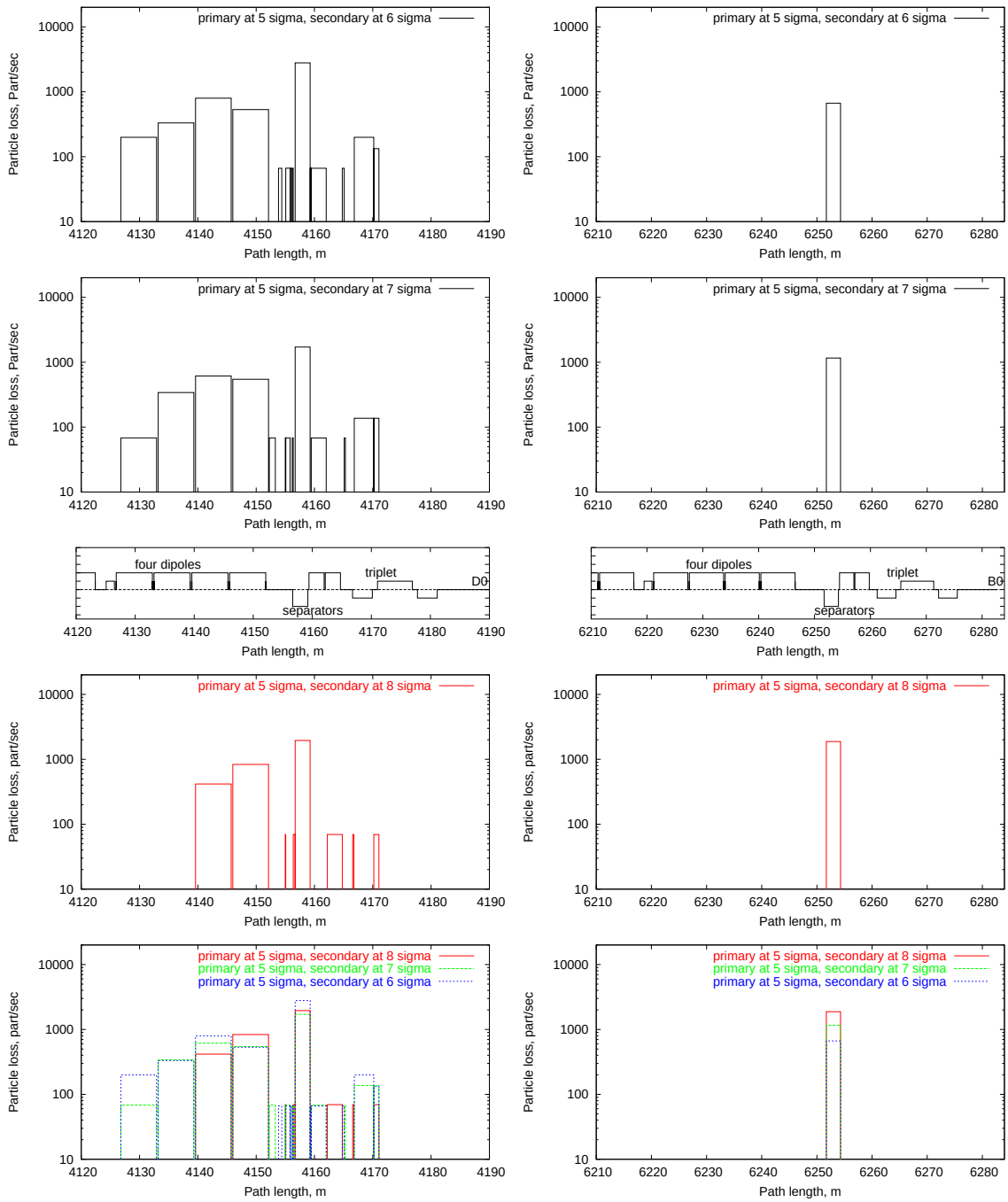

Figure 11: Beam loss distribution in the DØ and BØ regions for antiproton beam (second option) with secondary collimators offset with respect to the primary one of $1\sigma_{x,y}$ (top), $2\sigma_{x,y}$ (second line), $3\sigma_{x,y}$ (4-th line) and comparison of all cases (bottom).

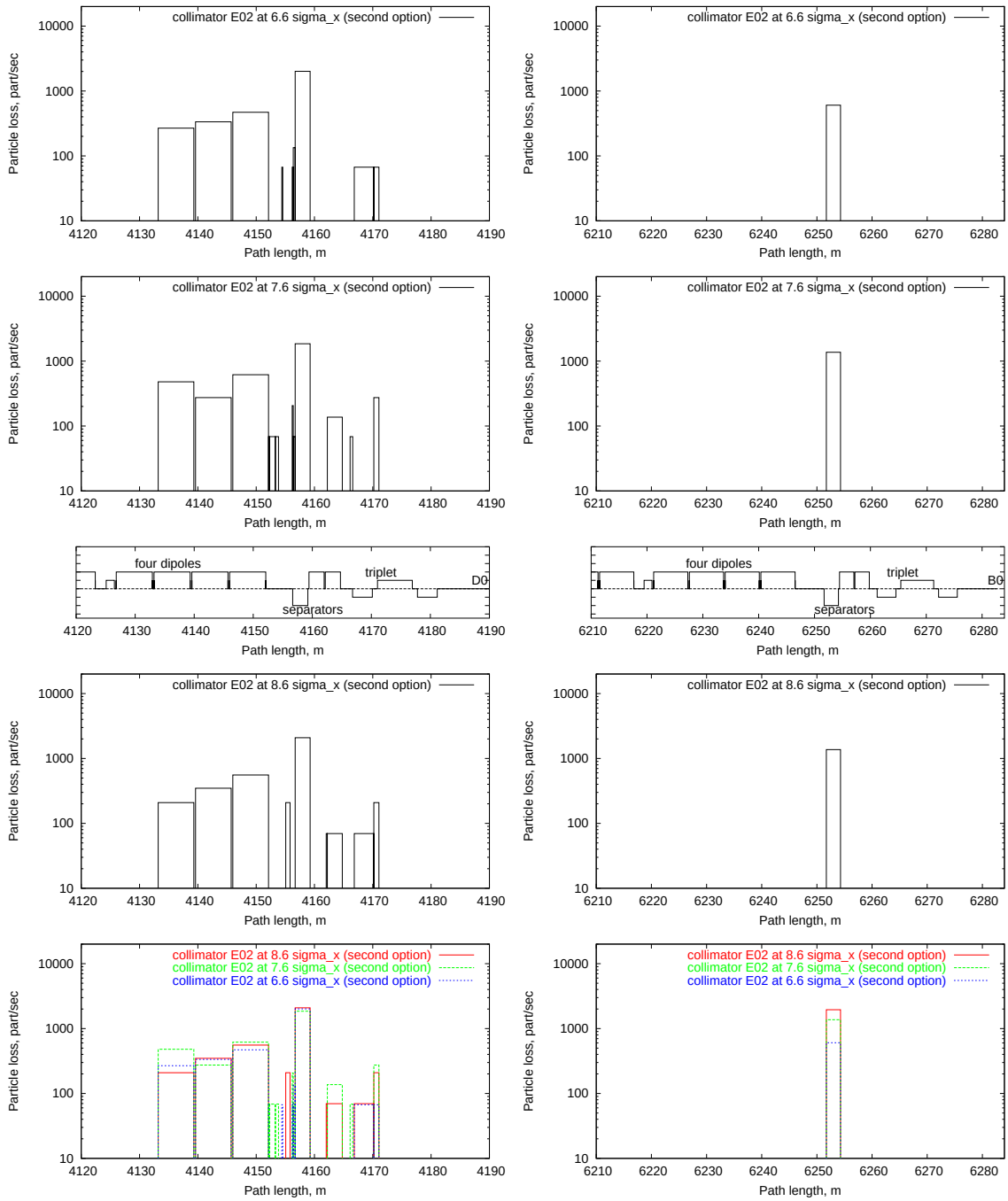

Figure 12: Beam loss distribution in the DØ and BØ regions for antiproton beam (second option) with secondary collimator F171 offset with respect to the primary one of $1\sigma_{x,y}$ (top), $2\sigma_{x,y}$ (second line), $3\sigma_{x,y}$ (4-th line), but with increased offset of the second secondary collimator E02 by $0.6\sigma_x$ and comparison of all cases (bottom). Increased offset of collimator E02 permits to decrease losses at this collimator, and at DØ region.

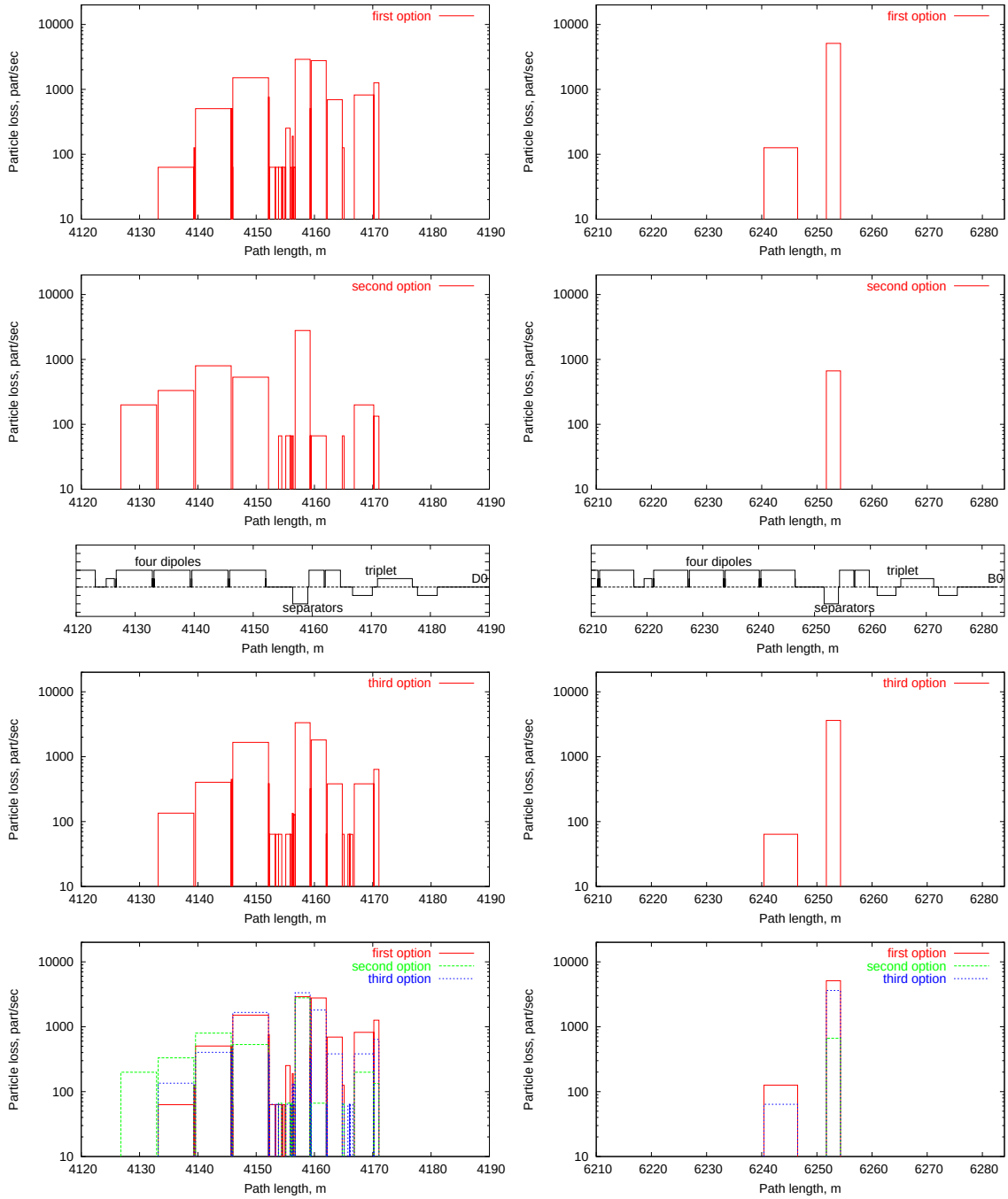

Figure 13: Beam loss distribution in the DØ (left) and BØ (right) regions for antiproton beam with primary collimators at $5\sigma_{x,y}$ and secondary collimators offset of $1\sigma_{x,y}$ with respect to the primary one. Top - first, middle - second and bottom - third option of collimation.

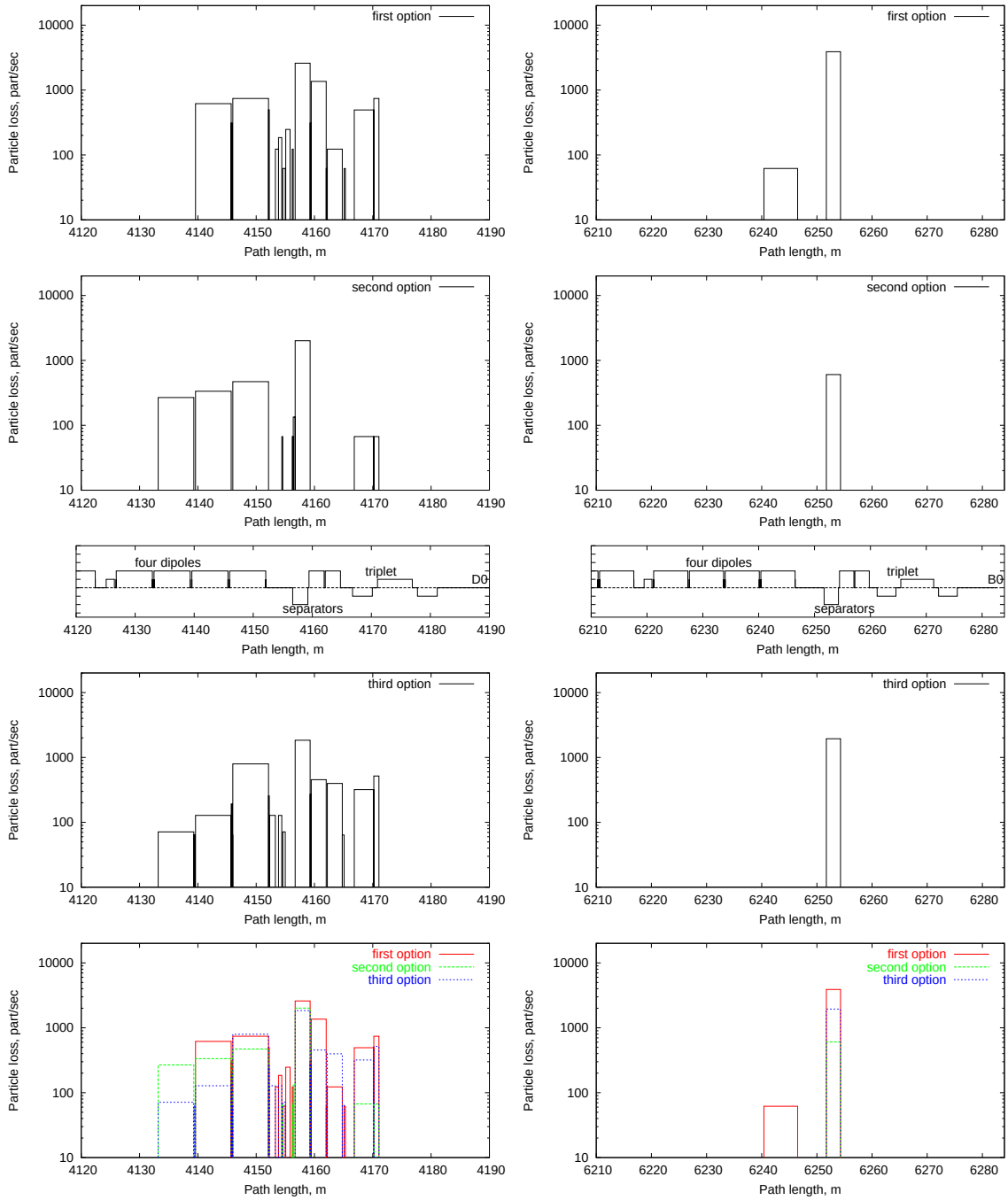

Figure 14: Beam loss distribution in the DØ (left) and BØ (right) regions for antiproton beam with primary collimators at $5\sigma_{x,y}$, first secondary collimator offset of $1\sigma_{x,y}$ and second secondary collimator offset of $1.6\sigma_{x,y}$ with respect to the primary one. Top - first, middle - second and bottom - third option of collimation.

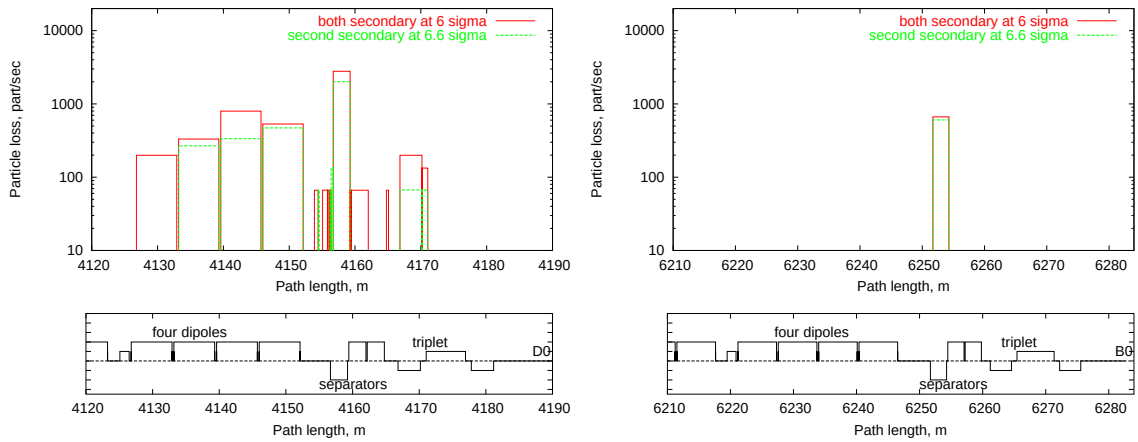

Figure 15: Beam loss distribution in the DØ (left) and BØ (right) regions for antiproton beam with primary collimators at $5\sigma_{x,y}$, secondary collimators offset of $1\sigma_{x,y}$ and second secondary collimator offset of $1.6\sigma_{x,y}$ with respect to the primary one for the second option of collimation.

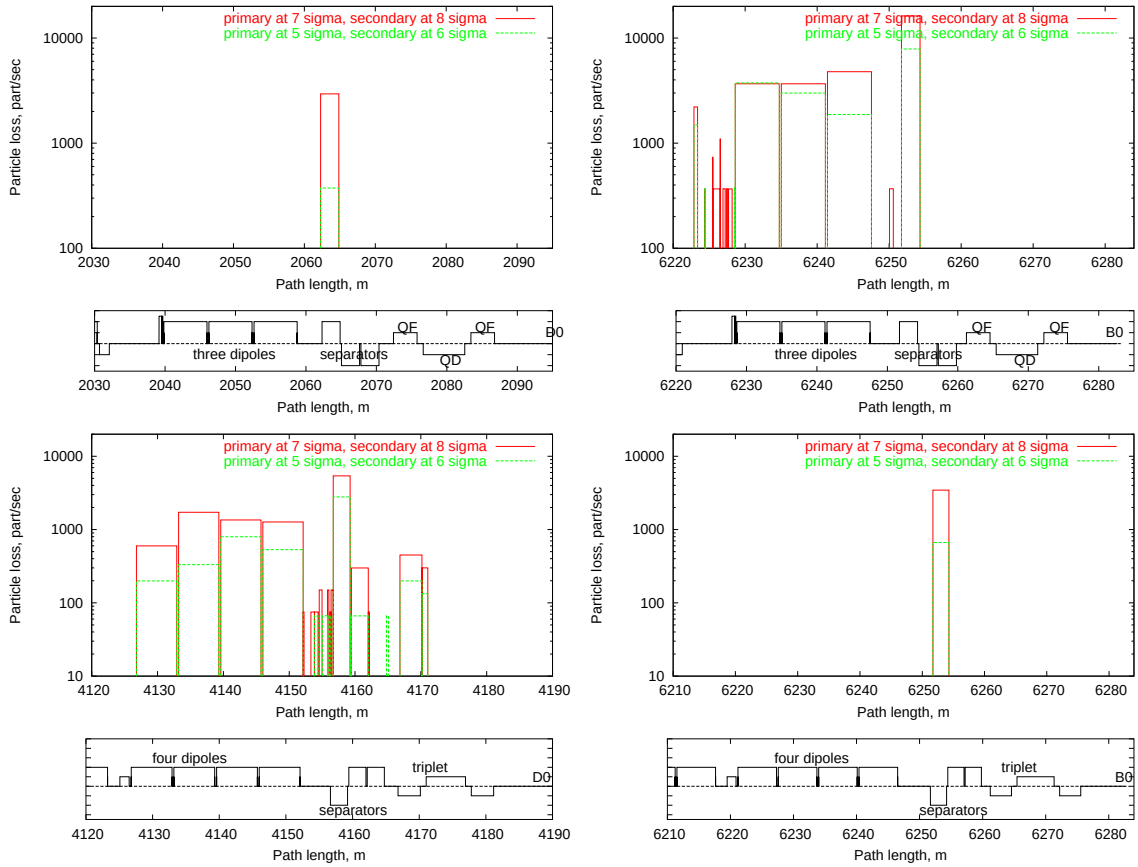

Figure 16: Beam loss distribution in the DØ (left) and BØ (right) regions for proton beam (top) and second option of antiproton collimation (bottom) with primary collimators at $5\sigma_{x,y}$ and secondary at $6\sigma_{x,y}$, and with all collimators retracted by 1 mm from this position.

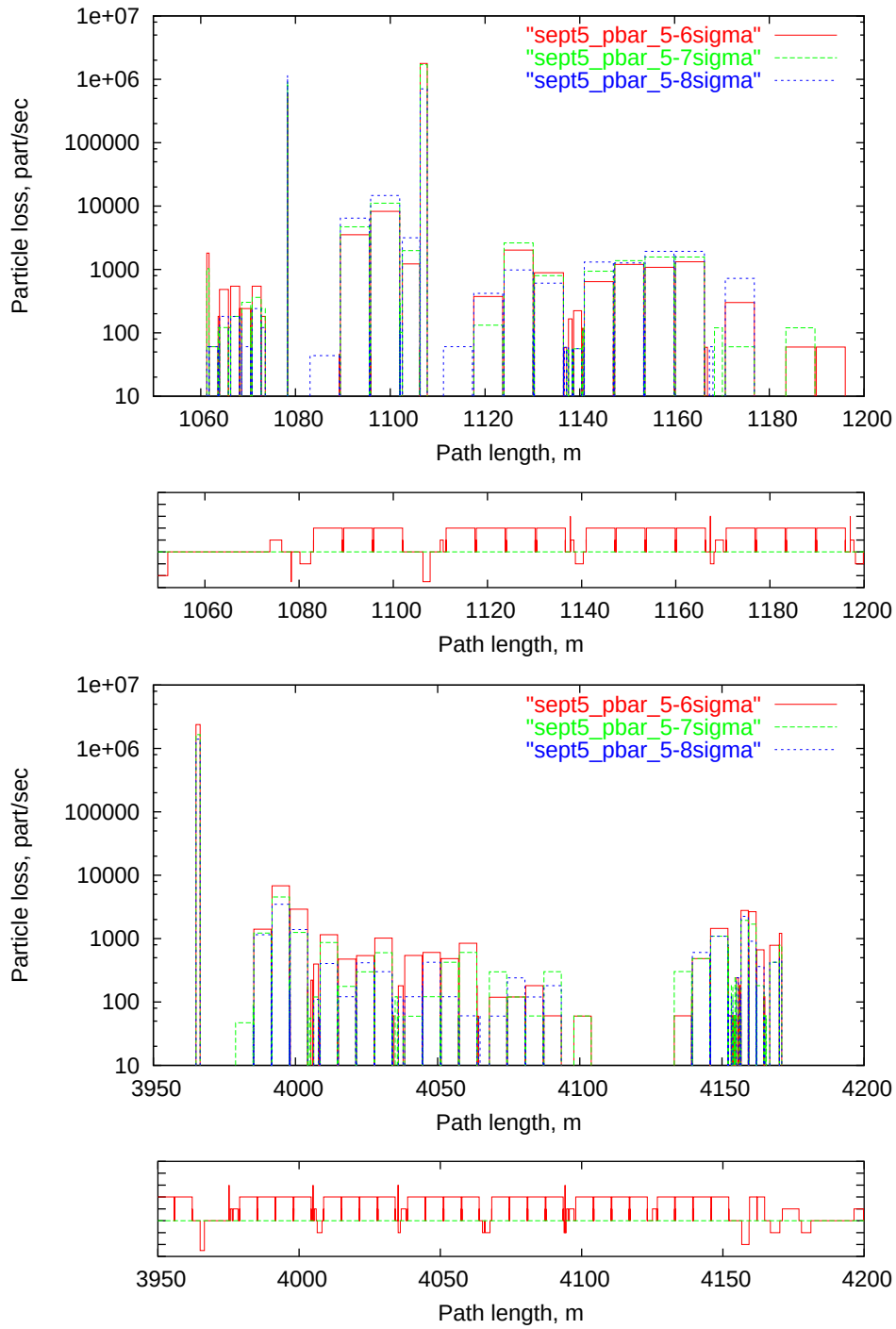

Figure 17: Beam loss distribution downstream of F49 (top) and D172 (bottom) antiproton collimators for different offset of secondary collimators.

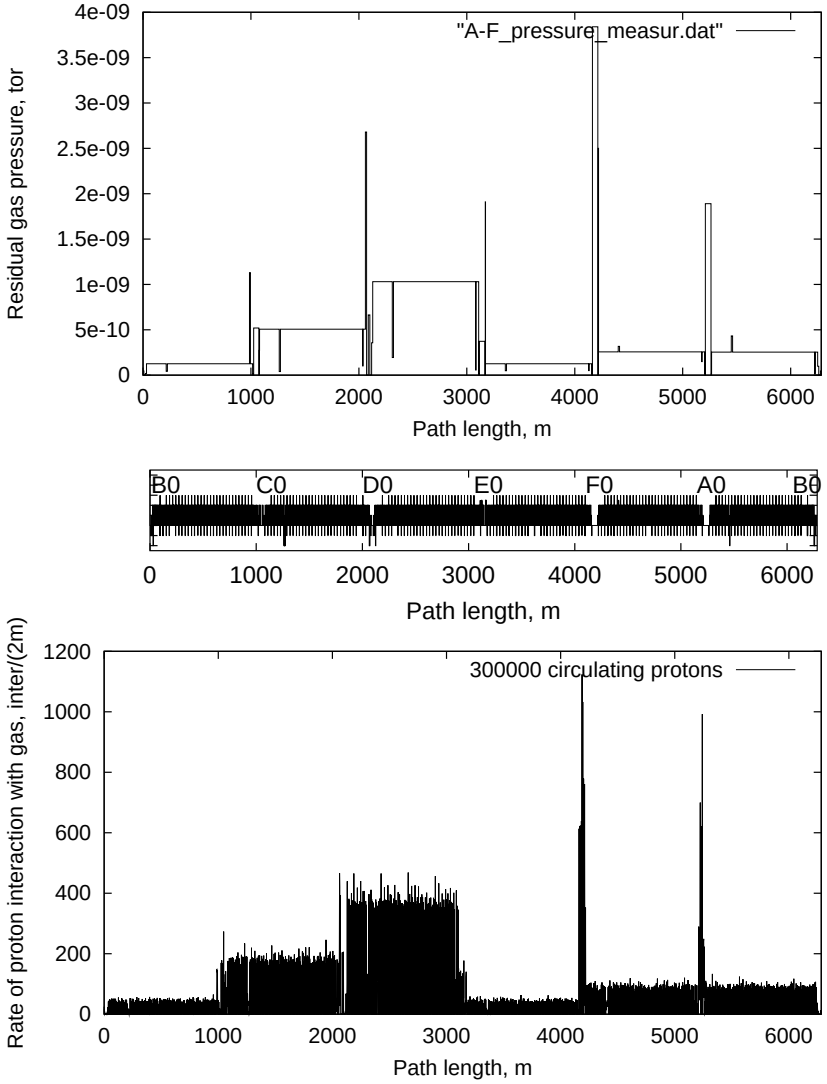

Figure 18: Measured residual gas pressure (top) and a calculated rate of proton nuclear elastic beam-gas interactions (bottom) in the Tevatron ring.

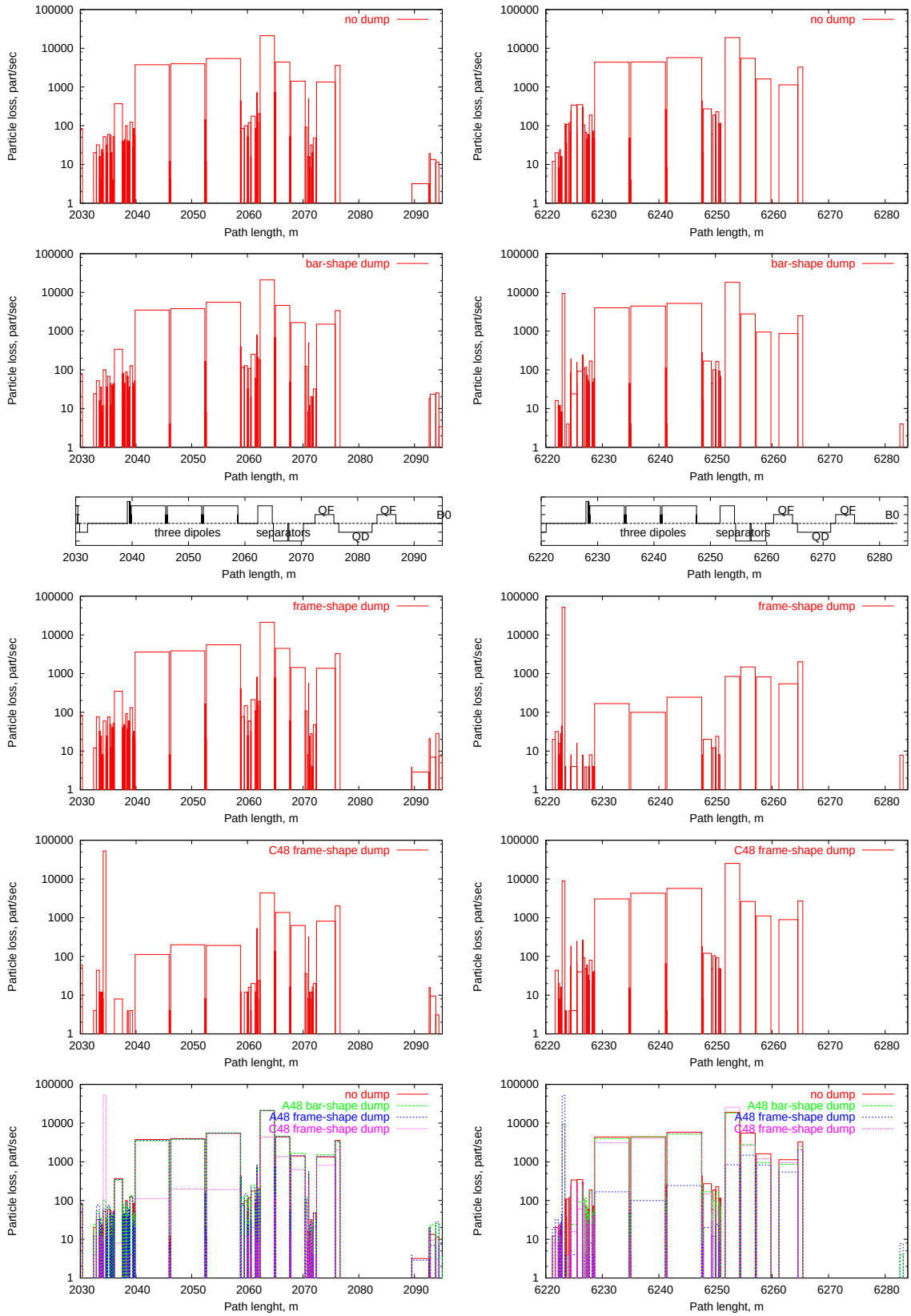

Figure 19: Beam loss distributions upstream of DØ (left) and BØ (right) for nuclear elastic beam-gas scattering of proton beam at measured gas pressure distribution. Top – without beam dump, second line – with bar-shape dump A48 at -20σ_y, 4-th line – with frame-shape dump A48 at $\pm 13\sigma_x, \pm 20\sigma_y$, 5-th line – with frame-shape dump C48 at $\pm 15\sigma_x, \pm 15\sigma_y$ and bottom – comparison of all cases of beam damp shape.

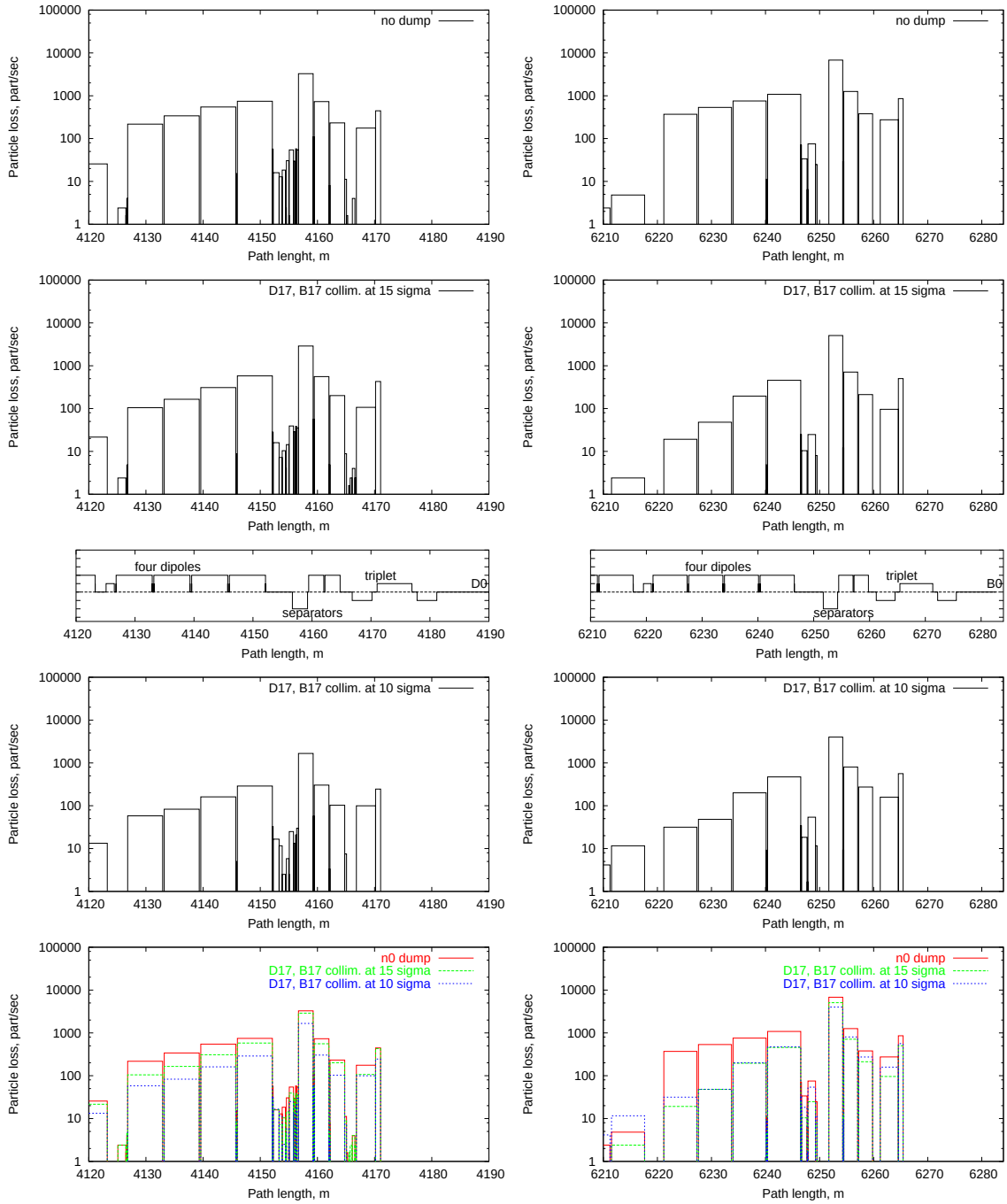

Figure 20: Beam loss distributions upstream of DØ (left) and BØ (right) for nuclear elastic beam-gas scattering of antiproton beam at measured gas pressure distribution. Top – without beam dump, second line – with two L-shape collimators at D17 and frame-shape collimator at B17 at $15\sigma_{x,y}$, 4-th line – with two L-shape collimators at D17 and frame-shape collimator at B17 at $10\sigma_{x,y}$ and bottom – comparison of previous cases.